European Journal of Radiology 91 (2017) 142–147

Contents lists available at ScienceDirect

European Journal of Radiology

journal homepage: www.elsevier.com/locate/ejrad

CT-based radiomics signature for differentiating Borrmann type IV gastric cancer from primary gastric lymphoma

Zelan Ma[a,1], Mengjie Fang[b,c,1], Yanqi Huang[a], Lan He[a,d], Xin Chen[e], Cuishan Liang[a,f], Xiaomei Huang[a,f], Zixuan Cheng[a,d], Di Dong[b,c], Changhong Liang[a], Jiajun Xie[e], Jie Tian[a,b,*], Zaiyi Liu[a,*]

[a] Department of Radiology, Guangdong General Hospital, Guangdong Academy of Medical Sciences, Guangzhou, 510080, China
[b] Key Laboratory of Molecular Imaging, Institute of Automation, Chinese Academy of Sciences, Beijing, 100190, China
[c] University of Chinese Academy of Sciences, Beijing, 100190, China
[d] School of Medicine, South China University of Technology, Guangzhou, Guangdong, 510006, China
[e] Department of Radiology, Guangzhou First People's Hospital, Guangzhou Medical University, Guangzhou 510180, China
[f] Southern Medical University, Guangzhou, Guangdong, 510515, China

ARTICLE INFO

Keywords:
Borrmann type IV gastric cancer
Primary gastric lymphoma
Computed tomography
Radiomics signature
Subjective CT findings

ABSTRACT

Purpose: To evaluate the value of CT-based radiomics signature for differentiating Borrmann type IV gastric cancer (GC) from primary gastric lymphoma (PGL).

Materials and methods: 40 patients with Borrmann type IV GC and 30 patients with PGL were retrospectively recruited. 485 radiomics features were extracted and selected from the portal venous CT images to build a radiomics signature. Subjective CT findings, including gastric wall peristalsis, perigastric fat infiltration, lymphadenopathy below the renal hila and enhancement pattern, were assessed to construct a subjective findings model. The radiomics signature, subjective CT findings, age and gender were integrated into a combined model by multivariate analysis. The diagnostic performance of these three models was assessed with receiver operating characteristics curves (ROC) and were compared using DeLong test.

Results: The subjective findings model, the radiomics signature and the combined model showed a diagnostic accuracy of 81.43% (AUC [area under the curve], 0.806; 95% CI [confidence interval]: 0.696–0.917; sensitivity, 63.33%; specificity, 95.00%), 84.29% (AUC, 0.886 [95% CI: 0.809–0.963]; sensitivity, 86.67%; specificity, 82.50%), 87.14% (AUC, 0.903 [95%CI: 0.831–0.975]; sensitivity, 70.00%; specificity, 100%), respectively. There were no significant differences in AUC among these three models (P = 0.051–0.422).

Conclusion: Radiomics analysis has the potential to accurately differentiate Borrmann type IV GC from PGL.

1. Introduction

The two most common gastric malignancies gastric cancer (GC) and primary gastric lymphoma (PGL) have markedly different management strategies, and the latter has a better prognosis [1]. Unlike GC, radiation or chemotherapy alone might be the best option for advanced PGL [2]. Thus, accurate differentiation of GC from PGL is important for determining the therapeutic strategy.

Endoscopic biopsies are generally thought to provide a reliable diagnosis. However, some reports have revealed that the yield is especially poor for the detection of lesions located predominantly in the submucosa, in which high false-negative rate can occur in the initial endoscopy/biopsy results, especially in the diagnosis of Borrmann type IV GC and PGL [1,3]. Although endoscopic ultrasound can reduce the misdiagnosis rate, a large and deep biopsy may produce a risk of perforation [4].

In clinical practice, noninvasive imaging modalities play an important role in the diagnosis and staging of gastric malignancies [5]. However, the differentiation of Borrmann type IV GC from PGL remains a diagnostic dilemma for radiologists [2,6]. Although some studies supported the utility of ^{18}F-fluorodeoxyglucose positron emission tomography (^{18}F-FDG PET)/computed tomography (CT) for distin-

* Corresponding authors at: Department of Radiology, Guangdong General Hospital, Guangdong Academy of Medical Sciences, 106 Zhongshan Er Road, Guangzhou 510080, China.
E-mail addresses: zelanma@163.com (Z. Ma), fmj5mj@gmail.com (M. Fang), yikiann@126.com (Y. Huang), helan0811@126.com (L. He), wolfchenxin@sina.com (X. Chen), liangcs2015@163.com (C. Liang), m18565253960@163.com (X. Huang), czxtlbb@126.com (Z. Cheng), di.dong@ia.ac.cn (D. Dong), cjr.lchh@vip.163.com (C. Liang), 904660014@qq.com (J. Xie), jie.tian@ia.ac.cn (J. Tian), zyliu@163.com (Z. Liu).
[1] These authors contributed equally.

http://dx.doi.org/10.1016/j.ejrad.2017.04.007
Received 3 March 2017; Received in revised form 7 April 2017; Accepted 9 April 2017

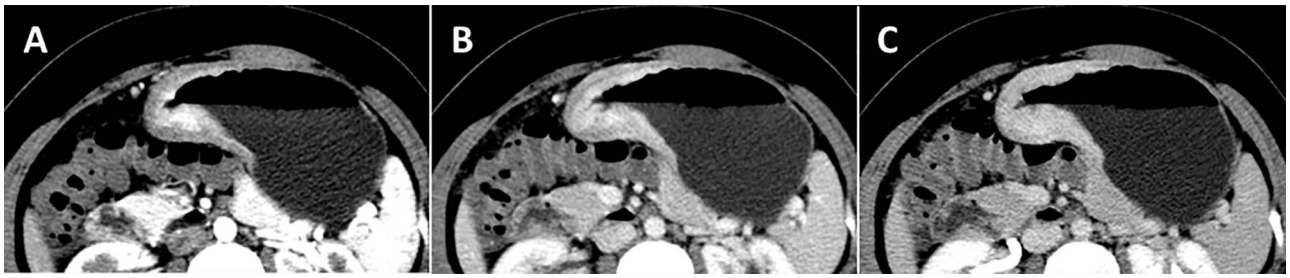

Fig. 1. Transverse CT scans in a 45-year-old man with Borrmann type IV AGC. A–C, Triple-phase contrast-enhanced images show thickened gastric wall with gradual inner to outer good transmural enhancement (Type A) from arterial to delayed phase. Perigastric fat planes are well maintained.

guishing GC from PGL [1,7], other studies proposed that its use in patients with indolent lymphomas should not be recommended due to their absence of FDG uptake [8,9]. CT is a common pretreatment examination for gastric malignancies [10], but it cannot reliably differentiate Borrmann type IV GC from PGL based on lesion distribution, wall thickness, and enhancement pattern, etc. [1,5].

Recently, the emerging field of radiomics has expanded its utilization and improved the understanding of imaging [11,12]. Radiomics is the process of extracting quantitative features from radiological images via a high-throughput analysis and selecting features to build a signature for a complete characterization of the tumours [13–15]. To the best of our knowledge, only one study [16] has explored a texture-based classification of different gastric tumours. However, this study only included 8 patients with PGL, and the results were obtained based on a 2-dimensional (2D) analysis, which may not provide a comprehensive view of the whole tumour.

Previous research has shown that radiomics can be a useful tool for differentiating fat-poor renal angiomyolipoma from renal cell carcinoma [17] and for differentiating prostate cancer from benign prostate tissue [18]. We hypothesized that radiomics could potentially add valuable information to differentiate Borrmann type IV GC from PGL by capturing more features beyond a visual interpretation. Therefore, we conducted this study to evaluate the value of a CT-based radiomics signature for differentiating Borrmann type IV GC from PGL.

2. Materials and methods

2.1. Patients

This retrospective study was approved by the institutional review board of our hospital, and informed consent was waived. From January 2011 to March 2016, 589 consecutive patients were pathologically diagnosed as PGL or Borrmann type IV AGC (advanced gastric cancer) in our hospital. The diagnosis of PGL was based on the fourth edition of the "WHO Classification of Tumours of Haematopoietic and Lymphoid tissues" [19]. The Borrmann classification was determined by the Japanese classification of AGC, according to the gross morphology of the pathology or operation data [20]. We excluded patients who did not have a pretreatment multiphasic dynamic CT in our hospital (n = 394); who with so unsatisfactory gastric distention that made it difficult to segment the tumour (n = 72); who with apparent distant metastases in AGC (n = 53), owing to its distant organ metastasis and metastatic lymphadenopathy were classically described as heterogeneous ring-enhancement, as well as the presence of peritoneal seeding, could be distinguished from PGL obviously [21].

2.2. CT image acquisition

All of the patients fasted for at least 5 h and were encouraged to drink 600–1000 ml water 30 min before the CT examination. CT was performed using a 64-channel (LightSpeed VCT, GE Healthcare, Milwaukee, WI) or an 8-channel multidetector CT scanner (Lightspeed Ultra, GE Healthcare, Hino, Japan). The CT scans, covering the entire stomach region, were acquired during a breath-hold with the patient supine in all of the phases. The imaging parameters were as follows: 120 kVp; 130 mAs; rotation time, 0.5 s; detector collimation, 64 × 0.625 mm or 8 × 0.625 mm; field of view, 350 × 350 mm; matrix, 512 × 512; and reconstruction section thickness, 1.25 mm.

Following a non-contrast enhanced CT, a contrast-enhanced CT was performed 25–30 s (arterial phase), 60 s (portal phase) and 180 s (delayed phase) after an infusion of 1.5 ml/kg of the iodinated contrast material (Ultravist 370, Bayer Schering Pharma, Berlin, Germany) with a pump injector (Ulrich CT Plus 150, Ulrich Medical, Ulm, Germany) at a rate of 3.5 ml/s into the antecubital vein.

2.3. Subjective CT findings evaluation

The subjective CT findings for each patient were independently evaluated and recorded in a blinded manner by two radiologists with 10 (Reader 1) and 8 years (Reader 2) of experience in the interpretation of abdominal CT. Inter-reader variability was evaluated. For the cases with a discrepancy in the subjective evaluation between the two readers, these were jointly reviewed by the two readers to reach a consensus for further analysis.

For imaging review, we first determined whether normal peristalsis of gastric wall during the period of scanning was present [22]. Second, we determined whether perigastric fat infiltration was present, which was defined as the outer gastric surface around the lesion exhibiting a lack of a clear perigastric fat plane [23]. Third, we defined lymphadenopathy below the renal hila as one of the short-axis diameters of the lymph nodes being larger than 8 mm in the corresponding region [23]. Additionally, we categorized the enhancement patterns into two types: Type A, a good gradual transmural tumour enhancement from the arterial to the delayed phase with thickened mucosal and submucosal layers and Type B, except the enhancement pattern of Type A [5]. Examples of these CT features were shown in Figs. 1 and 2.

2.4. Tumour imaging segmentation

To obtain the volume of interest (VOI) for further radiomics analysis, a manual segmentation was conducted with 3D Slicer software (version 4.3, http://www.slicer.org) on the portal venous contrast-enhanced CT images (thickness: 1.25 mm). The VOIs of the patients were contoured on the 2D image slices to include the entire tumour volume approximated by the two readers. Reader 1 performed tumours segmentations in all 70 patients, and Reader 2 performed tumours segmentations in 30 patients who were randomly selected from this cohort to assess inter-reader agreement of the radiomics analysis. We selected CT images on the portal venous phase for the tumour radiomics analysis because most of the gastric tumours had significantly enhanced tumour parts in this phase [10]. Contouring was drawn slightly within the borders of the tumour masses to avoid including adjacent air or fat [17]. The corresponding sagittal and coronal planes of the tumours could also be referenced when the lesion was ambiguous to be defined in the axial plane. An example of the manual segmentation was presented in Fig. 3.

Fig. 2. A 37-year-old female with primary gastric lymphoma. Diffuse wall thickening is presented from the body to the antrum on the same axial slice in the three contrast-enhanced phases. Gastric wall peristalsis is observed during the period of scanning (A–C). Perigastric fat planes are well maintained.

2.5. Radiomics feature extraction

The radiomics feature set used in this study contained 485 3D features, which contained 431 features from the study of Aerts et al. [11] and 54 additional modified phenotypic features designed and obtained by our group. The radiomics features can be divided into four groups: (I) first order statistics, (II) shape and size based features (including tumour volume), (III) texture features, (IV) wavelet features. Their extraction was performed in MATLAB 2014a (Mathworks, Natick, MA, USA). The additional modified features were described in Table 1.

3. Statistical analysis

3.1. Demographic characteristic of the patients

The differences in the age and gender between the two groups were assessed using an independent sample *t*-test and a Chi-square test, respectively.

3.2. Inter-reader agreement of the subjective findings evaluation and the radiomics features extraction

The inter-reader agreement of the evaluation of the subjective CT findings for all 70 patients was assessed with kappa statistics. A kappa value of 0.00–0.20 indicates poor agreement, 0.21–0.40 is fair, 0.41–0.60 is moderate, 0.61–0.80 is good, and 0.81–1.00 is excellent [10].

To estimate the reproducibility of the radiomics features extracted by the two radiologists from the independent segmentations of the CT images of 30 patients, the interclass correlation coefficient (ICC) was used. An ICC greater than 0.75 is regarded as being in good agreement [24].

3.3. Subjective findings model building

The differences in the subjective CT findings mentioned above between the two groups were analyzed using a Chi-square test or the Fisher's exact test, where appropriate. Subjective CT findings were combined to build the subjective findings model by multivariate logistic regression analysis, using the significant variables from the univariate analysis as inputs.

Table 1
Formulas used to calculate the Additional Modified Features.

Feature	Group	Formula
Standard Entropy	First order statistics	$entropy = -\sum_{i=1}^{N_l}\left(\frac{P(i)}{N}\right)\log_2\left(\frac{P(i)}{N}\right)$
Mass	First order statistics	The sum intensity value of X
Standard uniformity	First order statistics	$standarduniformity = \sum_{i=1}^{N_l}\left(\frac{P(i)}{N}\right)^2$
Mean	GLRLM-based features	$Mean = \frac{\sum_{i=1}^{N_g}\sum_{j=1}^{N_r} p(i,j\,\vert\,\theta)}{N_g N_r}$
Energy	GLRLM-based features	$Energy = \sum_{i=1}^{N_g}\sum_{j=1}^{N_r} p(i,j\vert\theta)^2$
Entropy	GLRLM-based features	$Entropy = -\sum_{i=1}^{N_g}\sum_{j=1}^{N_r} p(i,j\,\vert\,\theta)\log_2 p(i,j\,\vert\,\theta)$

Note.-X indicates the three dimensional image matrix with N voxels. P indicates the first order histogram divided by N_l discrete intensity levels. $p(i,j|\theta)$ indicates the (i,j)th entry in the given run-length matrix p for a direction θ. N_g is the number of discrete intensity values in the image. N_r is the number of different run lengths. N_p is the number of voxels in the image. As the three dimensional wavelet transform decomposes the original image into 8 decompositions and for each decomposition we computed the 6 features above, there are in total 54 additional modified phenotypic features in our study.

3.4. Radiomics feature selection and radiomics signature building

A Mann-Whitney *U* test was used to compare the value of each radiomics feature for the differentiation of Bormann type IV GC from PGL. The radiomics features, which met the criteria of being significantly different between the two groups and having an ICC greater than 0.75, were entered into the least absolute shrinkage and selection

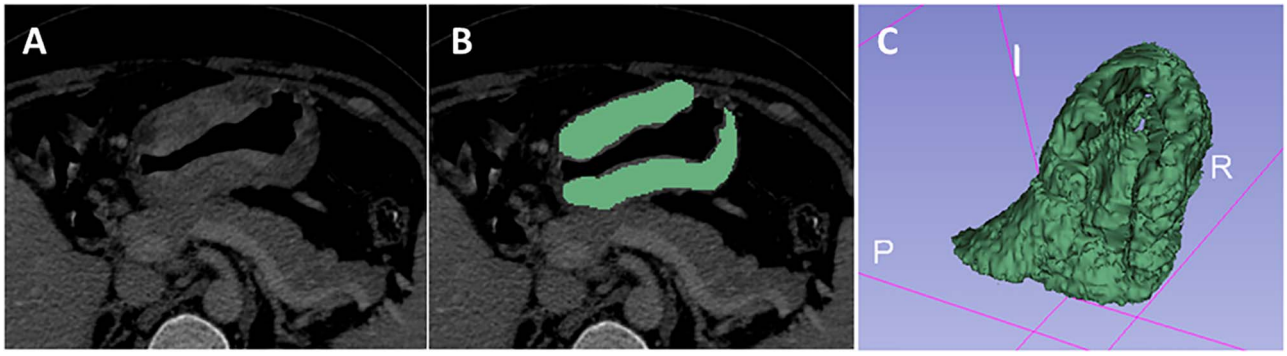

Fig. 3. An example of the manual segmentation in Borrmann type IV AGC. Diffusely infiltrating mass with heterogeneous enhancement is observed from the body to the distal antrum on the portal venous phase CT image (A). Manual segmentation on the same axial slice (B). 3D volumetric reconstructions of the tumour generated from 3D Slicer (C).

operator (LASSO) logistic regression model to select the most valuable features which is commonly applied in the regression of high-dimensional data [13,14,25]. The radiomics signature of each patient was built based on the LASSO-selected radiomics features and their respective coefficients. Borrmann type IV GC and PGL were entered into the model as 0 and 1, respectively. Difference in the radiomics signature between the two groups was analyzed by Mann-Whitney *U* test.

3.5. Development of the combined model incorporating with the independent pretreatment indicators

A prediction model integrating with the independent pretreatment indicators, which was referred as the combined model, was built with multivariable logistic regression analysis using the significant predictors from the univariate analysis as inputs. The likelihood ratio test with Akaike's information criterion was used as the stopping rule for a backward step-wise selection. The radiomics signature was entered into the logistic regression model as continuous variables, and the others were entered into the regression model as binary variables.

3.6. Diagnostic performance and inter-comparison of the subjective findings model, the radiomics signature and the combined model

Receiver operating curve (ROC) analysis was performed to determine the diagnostic performance of the subjective findings model, radiomics signature and the combined model with respect to the area under the curve (AUC), the sensitivity, the specificity and the accuracy. The cutoff value was selected to maximize the sum of the sensitivity and specificity values.

The classification generalizability and the performance of these models were evaluated by using a 7-fold cross-validation [26]. The differences in the AUC between the models were assessed using the Delong test [27].

All of the statistical computations and graphics were obtained in R 3.0.1 (http://www.Rproject.org). The LASSO logistic regression was performed using the "glmnet" package. The tests were two-tailed, and a value of $P < 0.05$ was considered statistically significant.

4. Results

4.1. Demographic characteristics of the patients

The patient cohort included 40 Borrmann type IV GC patients (13 males and 27 females; mean age, 57.38 ± 11.10 years; range, 38–84 years) and 30 PGL patients (19 males and 11 females; mean age, 55.23 ± 12.65 years; range, 24–85 years).

There was no significant difference in age between the two groups ($P = 0.680$), whereas gender was significantly different between the two groups ($P = 0.010$).

4.2. Inter-reader agreement of the subjective CT findings evaluation and the radiomics features extraction

The enhancement pattern showed excellent agreement, with a kappa value of 0.886 (95% CI [confidence interval]: 0.790–0.941). Evaluation of gastric wall peristalsis and lymphadenopathy below the renal hila showed good agreement, with kappa values of 0.798 (95% CI:0.689–0.875) and 0.718 (95% CI: 0.603–0.810), respectively. Perigastric fat infiltration showed moderate agreement, with a kappa value of 0.421 (95% CI: 0.313–0.538).

Of the 485 extracted radiomics features, 439 were demonstrated to have a good inter-reader agreement, with ICCs from 0.751 to 0.999, whereas 46 radiomics features had ICCs lower than 0.75 (range: 0.014–0.743). Note that as one of the radiomics features, tumour volumes showed a good inter-reader agreement with an ICC of 0.845 (95% CI: 0.743–0.912).

Table 2
Comparison of the Subjective CT Findings between Borrmann type IV GC and PGL (n = 70).

Subjective CT findings	Borrmann type IV GC	PGL	P Value
Gastric wall peristalsis			
Present	15 (37.5)	22 (73.3)	0.006
Absent	25 (62.5)	8 (26.7)	
Perigastric fat infiltration			
Present	21 (52.5)	10 (33.3)	0.176
Absent	19 (47.5)	20 (66.7)	
Lymphadenopathy below the renal hila			
Present	2 (5)	6 (20)	0.116
Absent	38 (95)	24 (80)	
Enhancement pattern			
Type A	28 (70)	7 (23.3)	< 0.001
Type B	12 (30)	23 (76.7)	

Note.-Numbers in parentheses are percentages. GC: gastric cancer. PGL: primary gastric lymphoma. Type A means good gradually transmural tumour enhancement from arterial to delayed phase with thickened mucosal and submucosal layers; Type B refers to the enhancement pattern except Type A.

4.3. Subjective findings model building

Absence of gastric wall peristalsis and the enhancement pattern of the Type A were significantly associated with Borrmann type IV GC ($P = 0.006$ and $P < 0.001$, respectively). With regard to perigastric fat infiltration and lymphadenopathy below the renal hila, there were no significant differences between Borrmann type IV GC and PGL (Table 2).

With multiple logistic regression analysis, gastric wall peristalsis (Odds ratio [OR], 0.206; 95% CI: 0.064,0.663) and the enhancement pattern (OR, 8.023; 95% CI: 2.495, 25.798) proved to be independent predictors in the subjective findings model.

4.4. Radiomics feature selection, radiomics signature building

A total of 183 radiomics signatures showed significant differences between Borrmann type IV GC and PGL ($p = 0.00001–0.05$), of which, 178 features with ICCs greater than 0.75 were entered into the LASSO logistic regression model to select the most valuable features. Tumour volume showed no significant difference between these two tumours and was not entered into the model. Finally, the radiomics signature was built using two features: [1] first order statistics − root_mean_square, which tends to emphasize the regions with high intensity levels; [2] HLH_GLCM (gray-level co-occurrence matrix) − sum_variance, which tends to emphasize the intensity patterns in the image. The radiomics signature score (Rad-score) was calculated using the following formula:

$$\text{Rad} - \text{score} = -8.070114381 - 0.005793309 \times \text{fosrootmeansquare} + 0.028721177 \times \text{HLHGLCMsumvariance}$$

The Rad-score showed statistically significant differences between Borrmann type IV GC and PGL (median GC: −0.389, interquartile range: [−0.432, −0.320]; median PGL: −0.187, interquartile range: [−0.273, −0.045]; $P < 0.001$).

4.5. Combined model building

The significant predictors in the univariate analysis, including gender, gastric wall peristalsis and enhancement pattern and radiomics signature, were entered into the multivariate analysis to build the

Table 3
Multivariate Analysis of the Parameters in Distinguishing Borrmann Type IV GC from PGL.

Parameter	β	Odds Ratio (95% CI)	P
Intercept	4.812	–	< 0.001
Radiomics signature	15.208	31.079 (5.597–172.590)	< 0.001
Absence of Gastric wall peristalsis	−1.656	0.191 (0.045–0.818)	0.026

Note.-β: the regression coefficient. CI: confidence interval. GC: gastric cancer. PGL: primary gastric lymphoma.

combined model. Finally, the radiomics signature and gastric wall peristalsis were identified as independent indicators (Table 3).

4.6. Diagnostic performance and inter-comparison of the subjective findings model, radiomics signature and the combined model

Diagnostic performance for each model was summarized in Table 4. The subjective findings model showed relatively lower AUC, sensitivity, and accuracy compared to that of the radiomics signature and the combined model. Radiomics signature demonstrated both high sensitivity and specificity (86.67% and 82.50%). Additionally, the combined model achieved a highest AUC (0.903) and an excellent specificity (100%). ROC curves of these three models were shown in Fig. 4.

However, there were no significant differences in AUC among these three models (the subjective findings model *vs* the radiomics signature, P = 0.188; the subjective findings model *vs* the combined model, P = 0.051; the radiomics signature *vs* the combined model, P = 0.422).

The cross-validation AUC achieved with each model were listed in Table 4. Delong test showed differences in AUC through pairwise comparison were not statistically significant (P = 0.065–0.279).

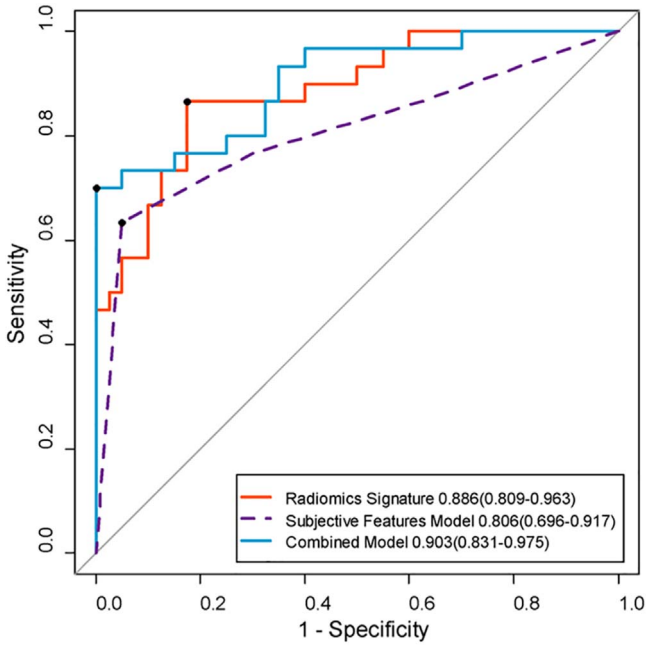

Fig. 4. Receiver operating characteristic (ROC) curves for the radiomics signature (red solid line), the subjective findings model (purple dashed line) and the combined model (blue solid line) in the differentiation of Borrmann type IV gastric cancer from primary gastric lymphoma. The solid dots represent the optimal cutoff values for the discrimination. The area under the curve (AUC) and 95% confidence inverval (CI) for the models are shown in the lower right corner of the figure.

5. Discussion

In this study, we developed a pretreatment CT-based radiomics signature to distinguish Borrmann type IV GC from PGL with a satisfactory discriminatory performance. Our results indicated that radiomics analysis is a potentially useful adjunct for distinguishing these two malignancies.

Radiomics, which appears to offer robust imaging biomarkers and epitomizes the pursuit of precision medicine, has attracted increased attention in recent years [28]. Previous research has showed its potential capacity to capture useful information and to increase the diagnostic and prognostic power [13,14,17,18,29]. Currently, the practice of identifying tumours as VOIs and extracting radiomics features from them has been regarded as the core of radiology in oncology [28]. Our study demonstrated the potential for a volumetric CT-based radiomics signature to act as a reproducible imaging marker for an accurate differentiation of Borrmann type IV GC from PGL.

Though there were no significant differences in AUC between the three models through pairwise comparison, radiomics analysis remains a useful complimentary non-invasive tool in clinical practice. First, in this study, the combined model incorporating the radiomics signature and the subjective CT findings achieved a specificity of 100%, which indicated an excellent correct diagnosis rate of Borrmann type IV GC. Second, as a computer-aided and quantitative biomarker, the radiomics signature could help less experienced radiologists and minimize inter-observer variability in imaging diagnosis. In addition, radiomics analysis is performed on existing images without additional cost and thus has the potential for broader clinical use.

The false-negative endoscopic findings for PGL and Borrmann type IV GC could be attributed to sampling errors because these lesions are easy to misdiagnose when the biopsies sample only the surface tissue [30]. Though CT-based volumetric radiomics analysis is not expected to replace pathological diagnosis, as a noninvasive approach to provide a complete characterization of the tumour [28], it may improve the differentiation of Borrmann type IV GC from PGL when sampling is inconclusive.

Our study has some complementary points compared with other studies. First, this study is the first to use 3D radiomics features to distinguish submucosal malignancies that occur in the stomach. Previous studies have shown that 3D features improved the discrimina-

Table 4
Diagnostic Performance of Subjective Findings Model, the Radiomics Signature and the Combined Model.

Model	Cutoff	AUC (95% CI)	Sensitivity[a]	Specificity[a]	Accuracy[a]	Cross-validated AUC[b] (95% CI)
Subjective Findings model	0.622	0.806 (0.696–0.917)	63.33 (19/30)	95.00 (38/40)	81.43 (57/70)	0.748 (0.626 − 0.873)
Radiomics Signature	−0.289	0.886 (0.809–0.963)	86.67 (26/30)	82.50 (33/40)	84.29 (59/70)	0.827 (0.726 − 0.928)
Combined model	0.690	0.903 (0.831–0.975)	70.00 (21/30)	100.00 (40/40)	87.14 (61/70)	0.863 (0.773 − 0.953)

Note.-CI: confidence interval.
[a] Numbers in parentheses were used to calculate percentages.
[b] AUC of the models after 7-fold cross-validation.

tion accuracy compared with using 2D features [31–33] because the former takes all of the available slices into consideration and provides abundant information. Second, we extracted the features from the contrast-enhanced CT images rather than the non-enhanced CT images, which achieved an improved visualization of the tumour and revealed enhancement heterogeneity. Third, because the biomarkers should be robust and validated, the extracted features were prioritized according to their reproducibility, and only features with an ICC greater than 0.75 were selected for further analysis.

However, there were some limitations to this study. First, as a case-control study, diagnostic accuracy is overestimated, thus, prospective and external validation studies are required. Second, segmentation of the tumours with indistinct borders is challenging and contentious, though volumetric measurement of the segmented tumours showed good inter-reader agreement, we didn't compare the difference in the measurement of segmented area. Incorporating these two methods will improve evaluation of the reproducibility of segmentation [12,28]. Third, it is not yet known whether other phases, such as the arterial phase, can be used to differentiate these two gastric malignancies. Therefore, further studies are necessary to address this point. In addition, although our study highlight the potential of a radiomics signature to achieve an accurate diagnosis, the biologic radiomics-pathology correlations have yet to be identified in published studies. Clearly, further work is needed to better understand the potential mechanism.

In conclusion, we presented a CT-based radiomics signature for distinguishing Borrmann type IV GC from PGL, which is discriminative to yield good diagnostic accuracy. As a more objective alternative to the visible CT findings, quantitative radiomics analysis would be a complimentary tool to add the radiologist's arsenal.

Conflicts of interest

None.

We confirm that all the listed authors have participated actively in the study, and have read and approved the submitted manuscript. The authors do not have any possible conflicts of interest.

Acknowledgement

We want to acknowledge the National Natural Scientific Foundation of China (No. 81271569, U1301258 and 81601469) and the Scientific Research and Equipment Development Project of Chinese Academy of Sciences (No. YZ201457) for their support.

References

[1] L. Fu, H. Li, H. Wang, B. Xu, Y. Fan, J. Tian, SUVmax/THKmax as a biomarker for distinguishing advanced gastric carcinoma from primary gastric lymphoma, PLoS One 7 (12) (2012) e50914.
[2] N.G. Kelessis, P.P. Vassilopoulos, M.P. Bai, N.J. Agnantis, S.R. Avital, R.J. Rosenthal, Update of the role of surgery in the multimodal treatment of MALT gastric lymphomas, Anticancer Res. 22 (6b) (2002) 3457–3463.
[3] K. Jung, M.I. Park, S.E. Kim, S.J. Park, Borrmann type 4 advanced gastric cancer: focus on the development of scirrhous gastric cancer, Clin. Endosc. 49 (4) (2016) 336–345.
[4] A. Andriulli, S. Recchia, C. De Angelis, et al., Endoscopic ultrasonographic evaluation of patients with biopsy negative gastric linitis plastica, Gastrointest. Endosc. 36 (6) (1990) 611–615.
[5] C.Y. Chen, T.S. Jaw, D.C. Wu, et al., MDCT of giant gastric folds: differential diagnosis, AJR Am. J. Roentgenol. 195 (5) (2010) 1124–1130.
[6] S. Ghai, J. Pattison, S. Ghai, M.E. O'Malley, K. Khalili, M. Stephens, Primary gastrointestinal lymphoma: spectrum of imaging findings with pathologic correlation, Radiographics 27 (5) (2007) 1371–1388.
[7] C. Giraudo, M. Raderer, G. Karanikas, et al., 18F-Fluorodeoxyglucose positron emission tomography/magnetic resonance in lymphoma: comparison with 18F-Fluorodeoxyglucose positron emission tomography/computed tomography and with the addition of magnetic resonance diffusion-weighted imaging, Invest. Radiol. 51 (3) (2016) 163–169.
[8] J.W. Hwang, S.R. Jee, S.H. Lee, J.H. Kim, S.Y. Seol, S.M. Lee, Efficacy of Positron emission tomography/computed tomography in gastric mucosa-associated lymphoid tissue lymphoma, Korean J. Gastroenterol. 67 (4) (2016) 183–188.
[9] M. Hoffmann, K. Kletter, M. Diemling, et al., Positron emission tomography with fluorine-18-2-fluoro-2-deoxy-D-glucose (F^{18}-FDG) does not visualize extranodal B-cell lymphoma of the mucosa-associated lymphoid tissue (MALT)-type, Ann. Oncol. 10 (10) (1999) 1185–1189.
[10] D. Tsurumaru, M. Miyasaka, Y. Nishimuta, et al., Differentiation of early gastric cancer with ulceration and resectable advanced gastric cancer using multiphasic dynamic multidetector CT, Eur. Radiol. 26 (5) (2016) 1330–1337.
[11] H.J.W.L. Aerts, E.R. Velazquez, R.T.H. Leijenaar, et al., Decoding tumour phenotype by noninvasive imaging using a quantitative radiomics approach, Nat. Commun. 5 (2014) 4006.
[12] V. Kumar, Y. Gu, S. Basu, et al., Radiomics: the process and the challenges, Magn. Reson. Imaging 30 (9) (2012) 1234–1248.
[13] C. Liang, Y. Huang, L. He, et al., The development and validation of a CT-based radiomics signature for the preoperative discrimination of stage I-II and stage III-IV colorectal cancer, Oncotarget 7 (21) (2016) 31401–31412.
[14] Y.Q. Huang, C.H. Liang, L. He, et al., Development and validation of a radiomics nomogram for preoperative prediction of lymph node metastasis in colorectal cancer, J. Clin. Oncol. 34 (18) (2016) 2157–2164.
[15] T.P. Coroller, P. Grossmann, Y. Hou, et al., CT-based radiomic signature predicts distant metastasis in lung adenocarcinoma, Radiother. Oncol. 114 (3) (2015) 345–350.
[16] A. Ba-Ssalamah, D. Muin, R. Schernthaner, et al., Texture-based classification of different gastric tumors at contrast-enhanced CT, Eur. J. Radiol. 82 (10) (2013) e537–e543.
[17] T. Hodgdon, M.D. McInnes, N. Schieda, T.A. Flood, L. Lamb, R.E. Thornhill, Can quantitative CT texture analysis be used to differentiate fat-poor renal angiomyolipoma from renal cell carcinoma on unenhanced CT images? Radiology 276 (3) (2015) 787–796.
[18] A. Wibmer, H. Hricak, T. Gondo, et al., Haralick texture analysis of prostate MRI: utility for differentiating non-cancerous prostate from prostate cancer and differentiating prostate cancers with different Gleason scores, Eur. Radiol. 25 (10) (2015) 2840–2850.
[19] S. Tohda, Overview of lymphoid neoplasms in the fourth edition of the WHO classification, Rinsho Byori 60 (6) (2012) 560–564.
[20] Japanese classification of gastric carcinoma: 3rd English edition, Gastric Cancer 14 (2) (2011) 101–112.
[21] P. Nagpal, A. Prakash, G.S. Pradhan, et al., MDCT imaging of the stomach: advances and applications, Br. J. Radiol. (2016) 20160412.
[22] M.S. Levine, L. Pantongrag-Brown, N.S. Aguilera, J.L. Buck, P.C. Buetow, Non-Hodgkin lymphoma of the stomach: a cause of linitis plastica, Radiology 201 (2) (1996) 375–378.
[23] A.Y. Kim, H.J. Kim, H.K. Ha, Gastric cancer by multidetector row CT: preoperative staging, Abdom. Imaging 30 (4) (2005) 465–472.
[24] K.A. Busing, A.K. Kilian, T. Schaible, A. Debus, C. Weiss, K.W. Neff, Reliability and validity of MR image lung volume measurement in fetuses with congenital diaphragmatic hernia and in vitro lung models, Radiology 246 (2) (2008) 553–561.
[25] S. Mueller-Using, T. Feldt, F.S. Sarfo, K.A. Eberhardt, Factors associated with performing tuberculosis screening of HIV-positive patients in Ghana: LASSO-based predictor selection in a large public health data set, BMC Public Health 16 (1) (2016) 563.
[26] A. Lungu, A.J. Swift, D. Capener, D. Kiely, R. Hose, J.M. Wild, Diagnosis of pulmonary hypertension from magnetic resonance imaging-based computational models and decision tree analysis, Pulm Circ. 6 (2) (2016) 181–190.
[27] E.R. DeLong, D.M. DeLong, D.L. Clarke-Pearson, Comparing the areas under two or more correlated receiver operating characteristic curves: a nonparametric approach, Biometrics 44 (3) (1988) 837–845.
[28] R.J. Gillies, P.E. Kinahan, H. Hricak, Radiomics: images are more than pictures, they are data, Radiology 278 (2) (2016) 563–577.
[29] K.A. Miles, B. Ganeshan, M.R. Griffiths, R.C. Young, C.R. Chatwin, Colorectal cancer: texture analysis of portal phase hepatic CT images as a potential marker of survival, Radiology 250 (2) (2009) 444–452.
[30] M.S. Levine, V. Kong, S.E. Rubesin, I. Laufer, H. Herlinger, Scirrhous carcinoma of the stomach: radiologic and endoscopic diagnosis, Radiology 175 (1) (1990) 151–154.
[31] P. Georgiadis, D. Cavouras, I. Kalatzis, et al., Enhancing the discrimination accuracy between metastases, gliomas and meningiomas on brain MRI by volumetric textural features and ensemble pattern recognition methods, Magn. Reson. Imaging 27 (1) (2009) 120–130.
[32] F. Ng, R. Kozarski, B. Ganeshan, V. Goh, Assessment of tumor heterogeneity by CT texture analysis: can the largest cross-sectional area be used as an alternative to whole tumor analysis? Eur. J. Radiol. 82 (2) (2013) 342–348.
[33] Y. Xu, E.J. van Beek, Y. Hwanjo, J. Guo, G. McLennan, E.A. Hoffman, Computer-aided classification of interstitial lung diseases via MDCT: 3D adaptive multiple feature method (3D AMFM), Acad. Radiol. 13 (8) (2006) 969–978.